

https://doi.org/10.1070/QEL16638

Generation of double giant pulses in actively *Q*-switched lasers

A.P. Korobeynikova, I.A. Shaikin, A.A. Shaykin, I.V. Koryukin, E.A. Khazanov

Abstract. **Generation of a second giant pulse in a longitudinal mode neighbouring to the longitudinal mode possessing minimal losses is theoretically and experimentally studied in actively *Q*-switched lasers. A mathematical model is suggested for explaining the giant pulse generation in a laser with multiple longitudinal modes. The model makes allowance for not only a standing, but also a running wave for each cavity mode. Results of numerical simulation and data of experiments with a Nd : YLF laser explain the effect of second giant pulse generation in a neighbouring longitudinal mode. After a giant pulse in the mode with minimal losses is generated, the threshold for the neighbouring longitudinal mode is still exceeded due to the effect of burning holes in the population inversion spatial distribution.**

Keywords: *active Q-switching, giant pulse, post-pulse, spatial hole burning, running wave.*

1. Introduction

Solid-state *Q*-switched lasers are widely employed in science and technology. Many applications require the single-mode regime, which provides a smooth laser emission pulse with a Gaussian beam intensity profile distribution. Selection of transverse modes is not difficult, whereas longitudinal mode selection is the main problem in developing such lasers. There are many approaches for obtaining single-mode emission. Most of them are based on the mode selection by a Fabry–Perot interferometer (FPI). A high pump energy excess over the threshold value specific of the *Q*-switching regime requires FPIs with a narrow transmission spectrum, capable of providing a substantial loss difference for neighbouring cavity longitudinal modes. Nevertheless, even if the width of FPI transmission spectrum approximately equals the cavity mode distance, the double-mode oscillation regime may occur in the case of symmetrical positions of the two modes relative to the FPI maximal transmission. If the cavity length is unstable and randomly varies within the limits of half-wavelength, then the cavity modes shift relative to the FPI spectrum; thus, the double-mode emission may occur. A small instability of the optical cavity length is inevitable due to temperature variations in an active element (AE) and air, as well as due to some other factors.

There are many ways to realise the single-mode and single-frequency emission (see, for example, [1–9] and references therein). Most approaches are based on keeping the frequency of one of the cavity modes near the FPI maximal transmission by using a feedback and active control of the cavity length. The main problem in this case is obtaining actual information about cavity mode positions. For this purpose, in [4, 5] the FPI reflection coefficient is used, and in [6] free emission peak profiles are analysed. In [7, 8], the long-duration-pulse pumping (6 ms) is used for obtaining single-frequency emission. The method suggested in [9] monitors longitudinal mode positions relative to the FPI transmission maximum. The method is based on observing emission of the second giant pulse (post-pulse). The post-pulse, observed in a time instant after the main giant pulse terminates, gives a chance to obtain information about mutual dispositions of cavity longitudinal modes and the FPI transmission maximum. The post-pulse emission in a neighbouring longitudinal mode was experimentally observed in [9], where it was qualitatively explained based on the effect of burning holes in the spatial distribution of population inversion. After the main giant pulse has been formed, the AE comprises the domains (standing wave nodes), which did not participate in generating the main mode, and have the residual population inversion exceeding the threshold value for a neighbouring mode. The remaining population inversion makes it possible to generate a second giant pulse at a neighbouring longitudinal mode.

In the present work, we give a strict theoretical explanation of the post-pulse emission effect in actively *Q*-switched lasers. The mathematical model developed describes correctly the effect of burning holes in an AE and demonstrates relation between the post-pulse emission parameters and the conditions of FPI transmission for cavity eigenmodes. Dependences of a post-pulse amplitude and its delay relative to the main giant pulse are experimentally studied versus the loss difference for the two modes. The experimental results well coincide with theoretical predictions, demonstrate the possibility to compensate for variations of the cavity optical length in real time and prevent double-mode emission.

A.P. Korobeynikova, I.A. Shaikin, A.A. Shaykin, I.V. Koryukin, E.A. Khazanov Institute of Applied Physics, Russian Academy of Sciences, ul. Ul'yanova 46, 603950 Nizhny Novgorod , Russia; e-mail: shaykin@appl.sci-nnov.ru

Received 16 February 2018
Kvantovaya Elektronika **48** (4) 351–357 (2018)
Translated by N.A. Raspopov

2. Modelling emission dynamics of multimode *Q*-switched lasers

2.1. Model description

Dynamics of laser pulse generation and population inversion in an AE is described by the system of equations [10]:

$$\frac{dm_i}{d\tau} = Gm_i\left(g_i\int_{z_0}^{z_0+l} n\Psi_i^2(z)dz - 1 - \beta_i\right),$$
$$\frac{dn}{d\tau} = A - n\left(1 + \sum_{i=1}^{N_m} g_i m_i \Psi_i^2(z)\right), \quad (1)$$

where

$$\Psi_i(z) = \sqrt{2}\sin k_i z = \sqrt{2}\sin[(\pi/L)(q_0 + i - 1)z] \quad (2)$$

are eigenmodes of an open cavity without losses to the radiation output; $i = 1,2,\ldots,N_m$ is the longitudinal mode number; N_m is the number of modes; q_0 is the central mode number; m_i is the field intensity for the ith cavity mode normalised to the saturation intensity; k_i is the wave vector of the ith mode; n is the population inversion for AE lasing levels; $\tau = t/\tau_{21}$ is the time normalised to the relaxation time of population inversion for lasing levels τ_{21}; z_0 is the coordinate of the AE front face; l is the AE length; g_i is the ratio of the ith mode gain to that of the mode nearest to the line centre ($g_i \leqslant 1$); A is the pump parameter corresponding to the maximal possible population inversion;

$$G = \frac{\tau_{21}}{\tau_{ph}};$$
$$\tau_{ph} = \frac{\tau_c}{-\ln R_1 R_2} \quad (3)$$

is the cavity photon lifetime; $\tau_c = L_{opt}/c$; L_{opt} is the cavity optical length; c is the speed of light; R_1 is the reflection coefficient of the output mirror; R_2 is the effective reflection coefficient of the second mirror, which includes all the losses for the central mode; and β_i are additional losses of the ith mode relative to the central mode losses.

As a Q-switch we will consider a Pockels cell (PC). In (1), the losses for cavity modes β_i comprise the losses β_{PC} related to the PC and the additional losses for the ith mode $\Delta\beta_i$ relative to the losses of the central (first) mode β_1. Thus, we have

$$\beta_i = \beta_{PC}(\tau) + \Delta\beta_i, \quad (4)$$

where

$$\beta_{PC}(\tau) = \begin{cases}\beta_{PC} \text{ at } 0 < \tau < T',\\ 0 \text{ at } \tau > T';\end{cases}$$

and T' is the instant of PC triggering, which actually corresponds to that of the maximal intensity for an emission peak.

For excluding the spatial variable z and simplifying the model we separate the AE to layers in such a way that the thickness of each layer is less than the emission wavelength. In each layer, the wave functions Ψ_i are taken constant. For each layer, a variable $n_k(\tau)$ is introduced. Hence, the integral over z in (1) turns to a sum, and system of equations (1) looks as follows:

$$\frac{dm_i}{d\tau} = Gm_i\left\{g_i\Delta z\sum_{k=1}^{N_n} n_k\left[\sqrt{2}\sin\left(\frac{\pi}{L}(q_0 + i - 1)z_k\right)\right]^2 - 1 - \beta_{PC}(\tau) - \Delta\beta_i\right\},$$
$$\frac{dn_k}{d\tau} = A - n_k\left\{1 + \sum_{i=1}^{N_m} g_i m_i\left[\sqrt{2}\sin\left(\frac{\pi}{L}(q_0 + i - 1)z_k\right)\right]^2\right\}, \quad (5)$$

where n_k is the population inversion in the kth layer of the AE; z_k is the coordinate of the kth layer; and $\Delta z = \lambda/10$ is the layer thickness.

The model was simulated in MATLAB by a program capable of solving the system comprising several hundred thousand differential equations; in the calculations, the well-known fourth order Runge–Kutt method was used, which is a numerical method for solving the Cauchy problem for first-order ordinary differential equations and systems.

Importantly, the model described above is developed in the standing wave approximation. However, intensities of the waves running across the cavity to the right and left differ due to the radiation output from the cavity and due to the fact that the waves are amplified in different directions. Thus, instead of (2) we will write the cavity eigenwaves in the form

$$\Psi_i^2(z) = \frac{2\sqrt{R_1}}{R_1 + 1}\cos 2k_i z + 1$$
$$= \frac{2\sqrt{R_1}}{R_1 + 1}\cos\left\{2\left[\frac{\pi}{L}(q_0 + i - 1)\right]z\right\} + 1. \quad (6)$$

2.2. Determining constants corresponding to the experimental conditions

The modelling requires some parameters such as initial values of field intensities for modes, the pump parameter, and the losses introduced by various elements including FPI, PC, etc. Figure 1 presents a schematic of the laser; its operation is thoroughly described below.

Part of horizontally polarised emission, which is not extracted from the cavity by a polariser, that is, the intensity transmission coefficient of the optical shutter is

$$T_{PC} = \cos^2\left(\frac{U}{U_{\lambda/4}}\frac{\pi}{2}\right), \quad (7)$$

where U is the voltage across the PC; and $U_{\lambda/4}$ is the quarter-wave voltage, that is, the voltage corresponding to the polarisation vector turn by $\pi/2$ after a linearly polarised wave twice passes the PC. The coefficient responsible for the losses introduced by the shutter is

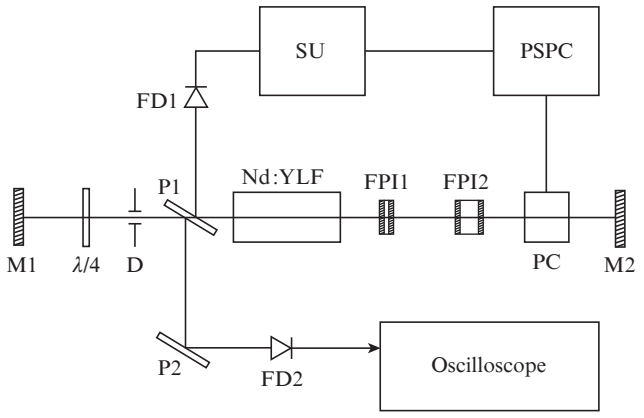

Figure 1. Schematic of the laser:
(M1, M2) mirrors; (D) diaphragm; (P1, P2) polarisers; (Nd:YLF) active element; (FPI1, FPI2) Fabry–Perot interferometers with the surface reflection coefficients of ~66% and bases of 3 and 15 mm; (PC) Pockels cell; (SU) synchronising unit; (PSPC) power supply for the Pockels cell; (FD1, FD2) fast diodes triggering the PC and oscilloscope.

$$\beta_{PC} = \frac{\ln T_{PC}}{\ln R_1 R_2}. \quad (8)$$

All other cavity losses for the central mode (except for those related to the radiation output from the cavity), which comprise transmission of the FPI and other elements, beam formation by a diaphragm, and so on, are included into the effective reflection coefficient of the second mirror:

$$R_2 = T_{FP} T_{pol1}^2 T_{pol2}^2 T_{AR}^{10} T_{dif} R_{mir}^2, \quad (9)$$

where T_{FP} is the transmission coefficient of two FPIs in double pass for the central mode; T_{pol1} and T_{pol2} are the transmission coefficients of two faces of the polariser P1 for the horizontal polarisation; T_{AR} is the transmission coefficient for surfaces of all optical elements comprised in the installation; T_{dif} is the diaphragm transmission coefficient; and R_{mir} is the reflection coefficient for the cavity mirrors M1 and M2.

The pump parameter A was chosen in such a way that the amplitude ratio of the giant pulse and free generation peak be equal to the experimentally measured value of 150. Note that the pump parameter should provide an excess of the population inversion over the threshold value for a neighbouring cavity longitudinal mode; otherwise, the second giant pulse fails to develop.

Radiation losses introduced by two FPIs are determined by transmission coefficients of the latter T_{FP}. In the simplest case, the transmission coefficient is calculated for the normal incidence of a plane wave onto the FPI ($\theta = 0$). A more precise calculation of the transmission coefficients for longitudinal modes requires taking into account the size of the incident beam and its intensity distribution. It was made by using the program written in the MATLAB environment, which calculates the coefficients taking into account parameters of the input beam and the angle of its incidence onto the FPI. The beam parameters were found by measuring the radiation intensity distribution at the four distances from the output polariser P1, corresponding to the distances from both FPIs in both passes. Figure 2 presents calculated FPI transmission spectra. Note that the FPI transmission spectra obtained are substantially wider and the maxima of transmission coefficients are less than in the plane wave approximation, where these are equal to unity.

The dependence of the FPI transmission coefficient on frequency yields the values of T_{FP} for the central (first) mode and for other cavity longitudinal modes. Thus, one can find the value of additional losses $\Delta\beta_i$, which will be different depending on the positions of cavity eigenfrequencies relative to the transmission coefficient maximum.

We will assume that if the shutter is closed (the voltage across the PC is distinct from zero), then the threshold value of the population inversion is not attained for all modes except for two. We will only consider these two modes. The loss difference $\Delta\beta$ for these modes is calculated by the equation

$$\Delta\beta = \ln \frac{T_{FP}(2)}{T_{FP}(1)} \frac{1}{\ln(R_1 R_2)}, \quad (10)$$

where $T_{FP}(1)$ and $T_{FP}(2)$ are the sum transmission coefficients of two FPIs for the first and second modes, respectively. The

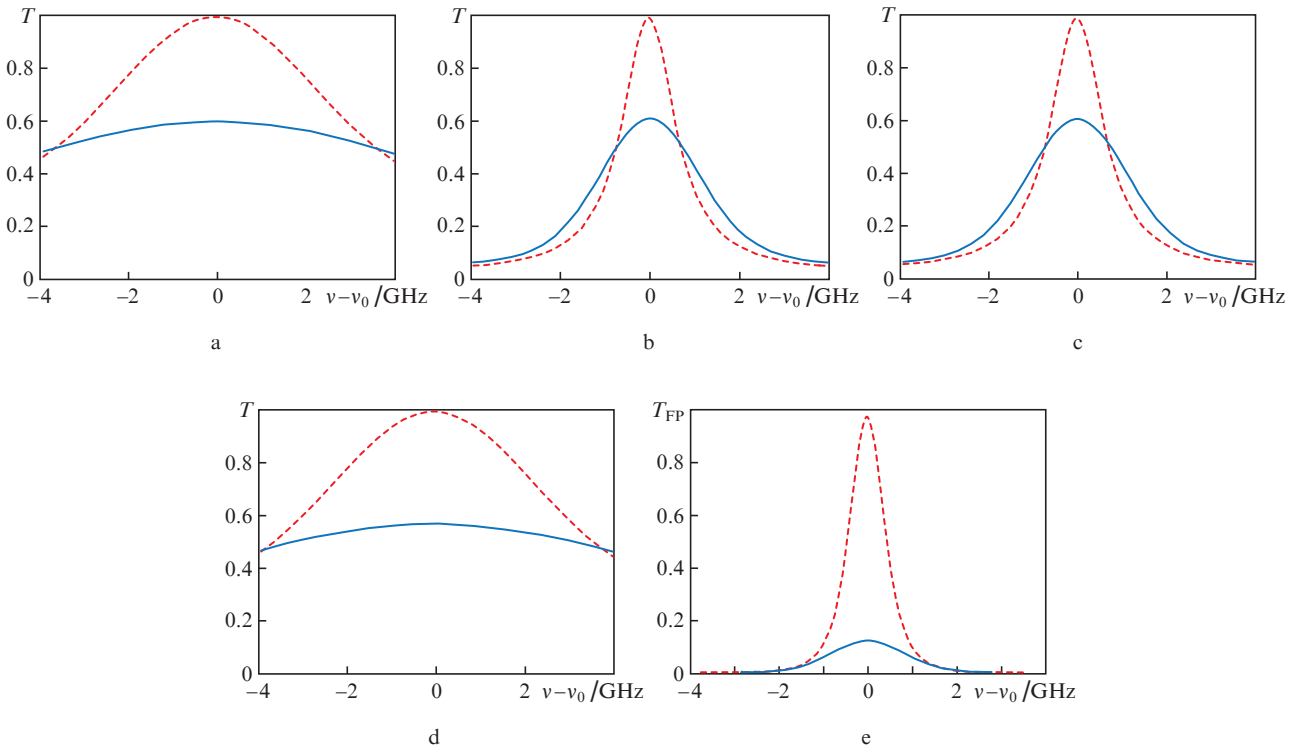

Figure 2. Dependence of the transmission coefficient on frequency after successive beam passage through interferometers (a, d) FPI1 at the incident angle of 0.003 rad and (b, c) FPI2 at the angle of 0.006 rad; (a, b) after the first transit and (c, d) after the second transit through the FPI, and (e) frequency dependences of the sum transmission coefficient T_{FP} for two interferometers after the radiation passes twice. Here, ν_0 is the frequency of the cavity central longitudinal mode, that is, the mode with minimal losses, for which FPI transmission is maximal. Dashed curves show FPI transmission spectra in the plane wave approximation.

value of $\Delta\beta$ varies depending on the cavity eigenfrequency positions relative to the curve $T_{FP}(\nu)$ (Fig. 2e). If the frequency of one longitudinal mode coincides with the transmission maximum (this case is shown in Fig. 2), then $\Delta\beta$ takes the maximal value equal to 0.021. If the mode frequencies are disposed symmetrically relative to the transmission maximum, then $\Delta\beta = 0$, that is, the emission conditions are equal for them and the double-mode regime is realised.

3. Modelling results

3.1. Post-pulse appearance

Emission was modelled for the parameters given in Table 1. First, the maximal value of $\Delta\beta$ was chosen for the central and neighbouring modes, then it reduced, which corresponded to a gradual shift of the cavity modes relative to the FPI transmission peak up to $\Delta\beta = 0$, where the conditions for mode development become equal.

Figure 3 presents pulses of free emission in the case of nonzero losses introduced by the PC at various values of $\Delta\beta$ for two central modes. In addition, the giant pulses developing after the cavity Q-factor is triggered, are shown. In the case where a frequency of one of the modes coincides with the FPI maximal transmission, the only pulse of free oscillation develops, which corresponds to this mode (Fig. 3a). Under Q-switching, a free generation pulse triggers the voltage across

Table 1. Parameters used in numerical simulation.

Parameters	Comments
$\beta_{PC} = 0.15$	Equation (8)
$R_1 = \cos^2 2\gamma = 0.52$	γ is the inclination angle of the quarter-wave plate
$R_2 = 0.1$	Equation (9) $T_{pol1} = 0.97$, $T_{pol2} = 0.98$, $T_{AR} = 0.996$, $R_{mir} = 0.995$, $T_{dif} = 0.99$, $T_{FP} = 0.365–0.370$
$\tau_c = 3.43 \times 10^{-9}$ s, $\tau_{ph} = 1.18 \times 10^{-9}$ s $\tau_{21} = 480 \times 10^{-6}$ s $A = 38.4$ $\Delta\beta = 0–0.021$	Equation (3)
$m_{i0} = \dfrac{\sigma}{\pi(d/2)^2} = 1.53 \times 10^{-17}$	m_{i0} is the intensity of noise spontaneous emission in the ith mode normalised to the saturation intensity, σ is the stimulated emission cross section, and d is the beam diameter

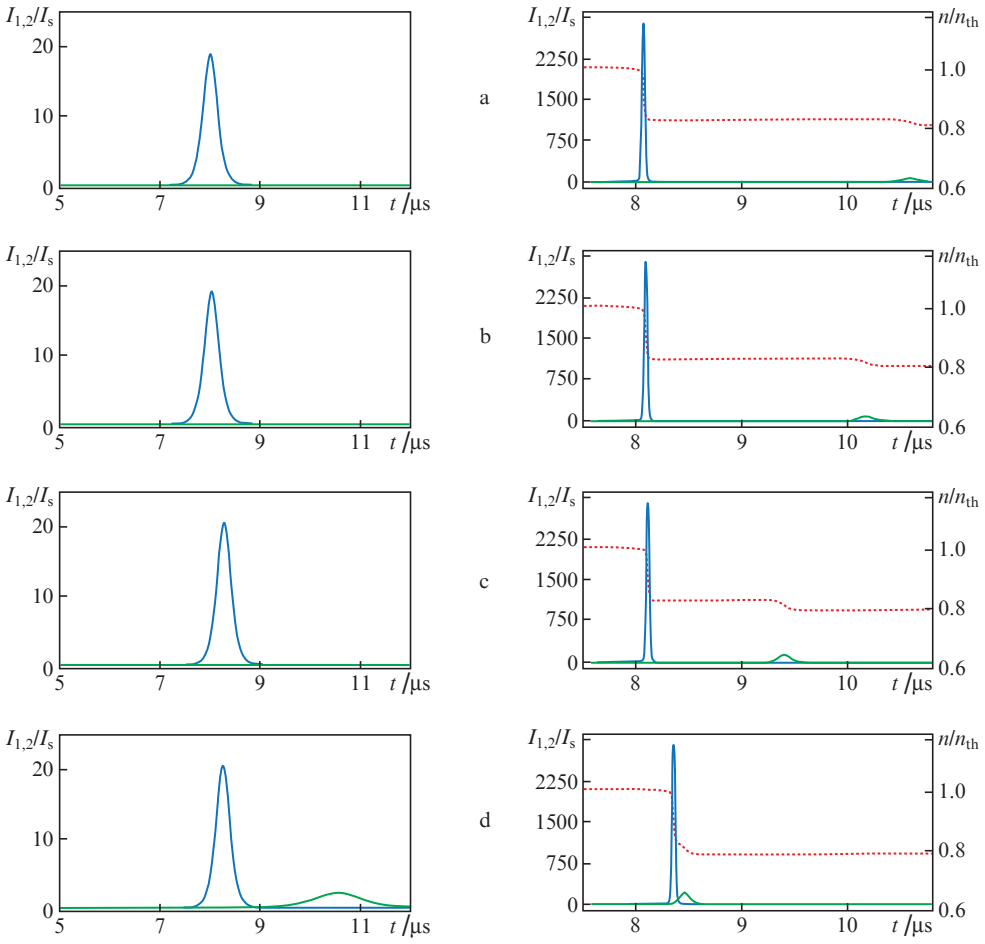

Figure 3. Results of modelling free emission pulses at nonzero losses introduced by the PC and the values of $\Delta\beta$ equal to (a) 0.021, (b) 0.017, (c) 0.008, and (d) 0.001 for two central modes; giant pulses, which develop when the cavity Q-factor is triggered, and the corresponding dependences $n/n_{th}(t)$ (dotted curves).

the PC. When the laser field intensity takes its maximum the cavity Q-factor changes and the losses β_{PC} turn to zero. At this instant, the losses of both modes become substantially less than the initial losses; the threshold value of population inversion falls, and the excess of the population inversion over the threshold becomes substantial. Due to this excess, the main giant pulse develops in the first mode, then a post-pulse is generated because the second mode gradually starts to develop. However, in contrast to the first mode, it starts from spontaneous noise at the instant of Q-switching, whereas the initial intensity of the first mode corresponds to the maximum of its free generation pulse. The post-pulse amplitude is substantially lower than that of the main giant pulse.

At a lower $\Delta\beta$, the conditions for neighbouring mode development become closer, the pulse at the second frequency begin to develop faster because its losses are smaller (Figs 3b–3d). The second mode starts to develop prior to Q-switching. Now, at the instant of PC opening, the intensity of the second mode exceeds the noise level. The time between the generation of the giant pulses decreases and finally they begin to partially and then completely overlap.

The modelling results described above have been obtained for the case where the AE is placed at the cavity centre. If the AE is near one of the mirrors, the post-pulse is actually never generated. There is a simple physical explanation. Due to the boundary conditions, all modes have nodes at the mirror; hence, the positions of nodes and antinodes in a standing wave are almost similar in two neighbouring modes and burning holes by emission of the first mode reduces the gain for not only the first mode, but for the second mode as well. Thus, after the main giant pulse has been formed, the residual population inversion is not sufficient for emitting a pulse at a distinct frequency. When the AE is placed at the cavity centre as in our case, the standing wave nodes for neighbouring modes are maximally separated in space and the population inversion for the second wave is high enough.

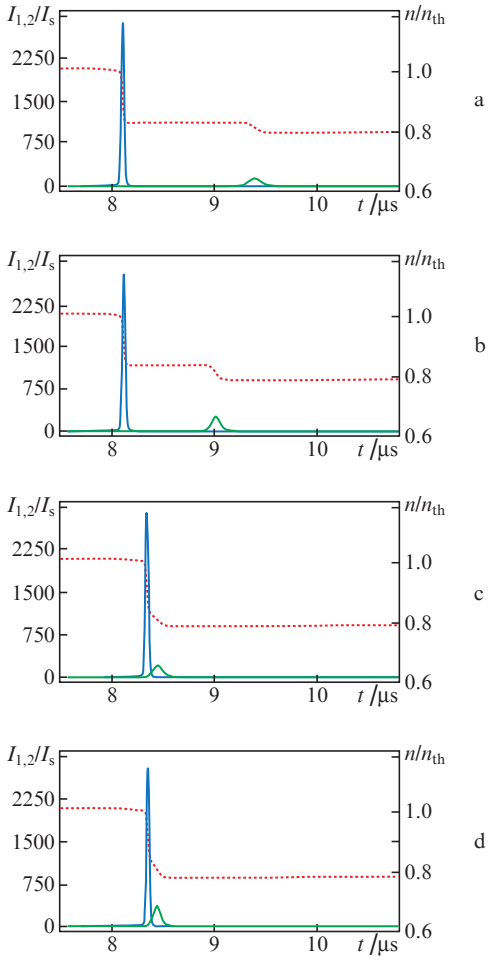

Figure 4. Modelling results for giant pulse generation (a, c) taking into account and (b, d) neglecting the running wave at $\Delta\beta$ equal to (a, b) 0.008 and (c, d) 0.001; the corresponding dependences $n/n_{th}(t)$ (dotted curves).

3.2. Taking into account a running wave

Let us compare modelling results for the two cases: cavity modes are presented as a purely standing wave (2) or as a superposition of a running and standing waves (6) (Fig. 4). In a solution comprising only standing waves there are domains in the AE, in which the first mode 'does not expend' the population inversion because its eigenfunction is zero in these domains. If a running wave is taken into account as well, such domains are absent. In this case, a small 'addition' of the running wave in the cavity makes the first mode to expend more efficiently the population inversion along the AE. Thus, the maximal amplitude of the main giant pulse is higher than without a running wave. Similarly, the second mode is partially amplified due to its 'running' component in the domains with a reduced inversion. In the result, the development of the post-pulse is delayed and its amplitude is lower, which is demonstrated in Fig. 4. However, we should note that with the cavity parameters used in the calculations, the picture does not change qualitatively and taking into account the component of a running wave yields only quantitative changes.

4. Experiment

In experiments, a master oscillator of the laser pumping an optical parametrical amplifier of chirped pulses in the PEARL petawatt laser complex was studied [11] (see Fig. 1). The laser cavity was formed by two highly reflecting mirrors separated by a distance of ~0.5 m. Polarised output radiation was provided by a polariser P1 and plate $\lambda/4$. The active element made of a Nd:YLF crystal (yttrium–lithium fluoride ($LiYF_4$) doped with neodimium) had the length of 75 mm, diameter of 5 mm, and neodimium ion concentration of 1.06%. It was placed inside a quantron case with two INP 5-75 lamps, a diffuse reflector, and a cooling system. The gain width for Nd:YLF is 1.4 nm. Transverse modes were selected by diaphragm D with a diameter of 1.7 mm, and longitudinal modes were selected by air Fabry–Perot interferometers FPI1 and FPI2 with surface reflection coefficients of ~66% and the lengths of 3 and 15 mm, respectively. The Q-switched operation was provided by a Pockels cell PC made of DKDP. Emission passing from the master oscillator has the following characteristics: the wavelength is 1054 nm, pulse duration is ~25 ns, its energy is ~8 mJ, and pulse repetition frequency is 1 Hz. Operation of this oscillator is more thoroughly described in [12].

The following experiment was carried out for observing generation of a post-pulse, obtaining the dependence of pulse generation time on the frequency shift of cavity modes and further comparison with results of mathematical simulation. One of the cavity mirrors was glued to a piezoceramic element that varied dimensions under applied constant voltage; thus,

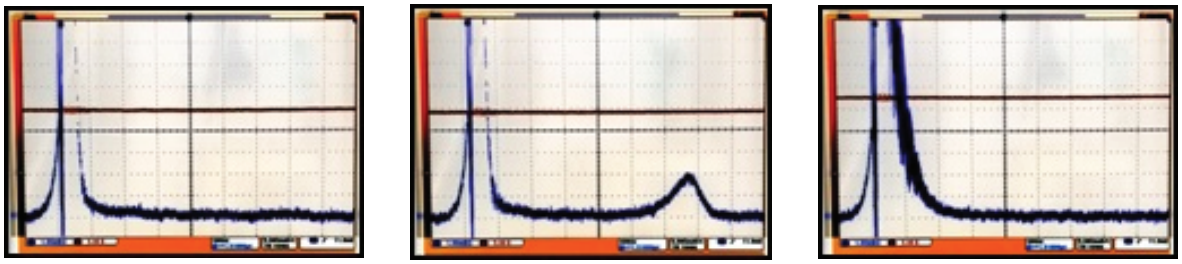

a b c

Figure 5. Oscillograms of laser emission pulses at voltages of (a) 12, (b) 15, and (c) 17 V across the piezoceramic element with a glued cavity mirror.

the cavity length was controlled. In this case, the frequencies of cavity eigenmodes shift relative to the FPI transmission peak, and emission conditions for neighbouring modes change. The variation of the voltage across the piezoceramic element by 11 V corresponds to a change in the cavity length L_{res} by 1 μm.

Oscillograms of laser emission pulses at the master oscillator output are shown in Fig. 5 for various voltage values. At the voltage of 12 V, a single-mode emission is observed (Fig. 5a); the post-pulse arises at a higher voltage (Fig. 5b), which approaches the main pulse and then interferes with the latter (Fig. 5c), that is, double-mode generation occurs. From the filling frequency of a fringe pattern, which is half the mode separation, one may conclude that emission occurs in two neighbouring longitudinal modes of the cavity.

The experimental dependences of the post-pulse time delay and its amplitude on the voltage applied to the piezoceramic element well agree with those calculated by the model described above (Fig. 6). Thus, we have experimentally and theoretically proved that appearance of the post-pulse in the *Q*-switching regime is related to worsening of longitudinal mode selection, which is related to burning holes in the population inversion of the AE.

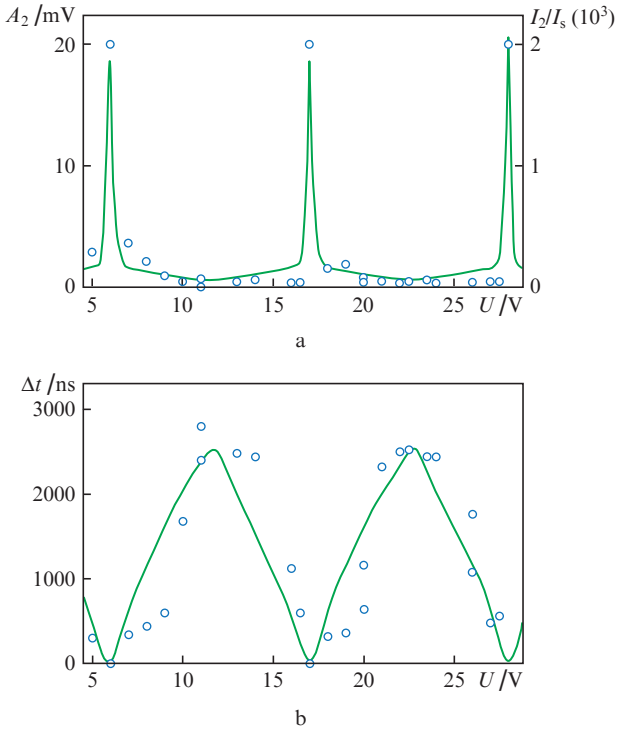

Figure 6. (a) Post-pulse amplitude and (b) delay time vs. the voltage across the piezoceramic element; solid curves correspond to theoretical results, points refer to experiments.

5. Conclusions

The work presents a mathematical model, which describes the development of multimode emission and evolution of population inversion in the AE of a *Q*-switched laser. For the first time the model takes into account not only a standing wave, but also a running wave for each longitudinal mode in the cavity. The numerical simulation and experiment show that generation of the second giant pulse (post-pulse) occurs in a neighbouring longitudinal mode due to the effect of burning holes in the AE population inversion distribution. At a sufficient difference in the losses for two neighbouring longitudinal modes, the post-pulse arises with a substantial time delay relative to the main giant pulse and its amplitude is small. At a smaller distinction, the delay reduces and the post-pulse amplitude increases. At a very small difference of losses, two giant pulses are actually simultaneously generated; it is a classical double-frequency generation, and the field intensity increases several-fold. This oscillation regime is quite undesirable because it increases manifold the probability of laser optical element breakdown. Detection of the post-pulse makes it possible to form a feedback signal for adjusting the cavity length in order to improve selection of longitudinal modes.

Acknowledgements. The work was supported by the Russian Science Foundation (Grant No. 17-72-20111). The laser stand was upgraded in the frameworks of the Programme for the Development of IAP RAS in 2016–2020 (Agreement No. 007-02-1225/2).

References

1. Yanovsky V.P., Richardson M.C., Miesak E.J. *IEEE J. Quantum Electron.*, **30**, 884 (1994).
2. Zhang J., Zhu X., Zang H., Ma X., Yin S., Li S., Chen W. *App. Opt.*, **53**, 7241 (2014).
3. Andreev N.F., Palashov O.V., Khazanov E.A. *Quantum Electron.*, **26**, 330 (1996) [*Kvantovaya Elektron.*, **23**, 338 (1996)].
4. Carr I.D., Hanna D.C., Wong K.-H. *Opt. Commun.*, **55**, 179 (1985).
5. Andreev N.F., Bondarenko N.G., Eremina I.V., Kuznetsov S.V., Palashov O.V., Pasmanik G.A., Khazanov E.A. *Quantum Electron.*, **21**, 1045 (1991) [*Kvantovaya Elektron.*, **18**, 1154 (1991)].
6. Hanna D.C., Koo Y.W.J. *Opt. Commun.*, **43**, 414 (1982).
7. Kuizenga D.J. *IEEE J. Quantum Electron.*, **17**, 1694 (1981).
8. Duvillier T., Luce J., Diard A. *Opt. Commun.*, **59**, 127 (1986).

9. Shaykin A.A., Burdonov K.F., Khazanov E.A. *Laser Phys. Lett.*, **12**, 125001 (2015).
10. Khanin Ya.I. *Osnovy dinamiki lazerov* (*Laser Dynamics Theory*) (Moscow: Nauka, 1999) pp 136–147.
11. Lozhkarev V.V., Freidman G.I., Ginzburg V.N., Katin E.V., Khazanov E.A., Kirsanov A.V., Luchinin G.A., Mal'shakov A.N., Martyanov M.A., Palashov O.V., Poteomkin A.K., Sergeev A.M., Shaykin A.A., Yakovlev I.V. *Laser Phys. Lett.*, **4**, 421 (2007).
12. Katin E.V., Lozhkarev V.V., Palashov O.V., Khazanov E.A. *Quantum Electron.*, **33**, 836 (2003) [*Kvantovaya Elektron.*, **33**, 836 (2003)].